STUDY OF MULTIPLE IMPACTS OF A RIGID BODY WITH A FLAT SURFACE

by

FLORIN VASILE BADIU

Presented to the Faculty of the Graduate School of

The University of Texas at Arlington in Partial Fulfillment

of the Requirements

for the Degree of

DOCTOR OF PHILOSOPHY

THE UNIVERSITY OF TEXAS AT ARLINGTON

December 2007

ACKNOWLEDGEMENTS

I thank first to my parents, for their constant support, guidance, and caring. I thank them in particular for their professional advices, my father being a Mathematician, and my mother a Teacher.

I thank all my Professors I had at UT-Arlington (2002-2007), and at University of Bucharest (1992-1997). I was lucky to have such good advisors as Dr. Jianzhong Su for my PhD and Dr. Irinel Dragan for my Master of Science at UT-Arlington, and Dr. Eugen Campu for my Bachelor of Science in Romania.

December 12, 2007

ABSTRACT

STUDY OF MULTIPLE IMPACTS OF A RIGID BODY WITH A FLAT SURFACE

Publication No. _____

FLORIN VASILE BADIU, Ph.D.

The University of Texas at Arlington, 2007

Supervising Professor: Jianzhong Su

Both analytical and numerical results are presented for two rigid body problems: a rod colliding with the ground, and a rigid thin plate colliding with the ground. The study of the succession of impacts of the rod with the ground confirms results from literature, and explores new cases. Numerical simulations can provide results in the study of the clattering impacts of a 3D body colliding with the ground. For a simplification of the analytical calculations, a rectangular plate without thickness is studied. In this case, a comparison between the numerical method, which is a continuous contact method, and the analytical method, which is a discrete method, is performed.

TABLE OF CONTENTS

LIST OF FIGURES

LIST OF TABLES

CHAPTER 1

INTRODUCTION

The *impact* is defined as a complex physical phenomenon, which occurs when two or more bodies collide with each other [22]. It is characterized by a very brief duration, high force levels reached, possibly rapid dissipation of energy, and large accelerations and decelerations. As a consequence, the bodies are subject to elastic or plastic deformation, with transfer of energy in various forms [9]. All these aspects must be considered while designing and analyzing a mechanical system [2]. A more generally defined concept is *contact*. Sometimes it is used interchangeably with impact. Impact is used more often for cases where there is only one impact point (or area), while contact is used more often in cases where there are two or more contact points (or areas) between the bodies that collide [8].

There are two approaches to treat the impact/contact problems. The first approach assumes an instant collision between the objects, with no or little change of local configurations of the bodies. The dynamic analysis is split in two phases: before impact, and after impact. During impact, slipping, sticking, or reverse motion may occur. While modeling the energy transfer and dissipation, various coefficients are being used, like the coefficient of restitution and the impulse ratio [3, 4]. These methods are called *impulse-momentum* or *discrete* methods [16], and are usually used for rigid body impacts. The second approach takes into account the fact that the interaction forces act continuously during the impact. In this case, the contact forces are added to the equations of motion during their action period. These methods are more suitable for contact modeling and multiple body contact. They are called *continuous analysis* or *force based* methods [16].

We define the *line of impact* as the normal line to the tangential plane at the contact point. According to the position of this normal line, four types of impact can be defined for single-point collision between two bodies: (a) *central* or *collinear*, if the mass centers of the two bodies are on the line of impact; (b) *eccentric* if the mass centers of one or both bodies are not on the line of impact; (c) *direct*, if the initial velocities of the two bodies are along the line of impact; (d) *oblique*, if the initial velocities of one or both bodies are not along the line of impact.

In the dynamics of impact, two phases can be identified. These are *compression* and *restitution*, as shown in Figure 1.1 [2, 3, 9, 34]. Compression starts when the two bodies come in contact at the instant t_0, and ends when the maximum deformation is reached at the instant t_m. Restitution starts at the instant t_m, and ends at the instant t_f, when the two bodies separate.

With respect to the energy loss, impact can be classified into: (a) *perfectly elastic*, line O-A-C, where no energy is lost; (b) *perfectly plastic*, line O-A, where all energy is lost and the deformation is permanent; (c) *partially elastic*, line O-A-D, with energy loss but no permanent deformation; (d) *partially plastic*, line O-A-B, with energy loss and permanent deformation.

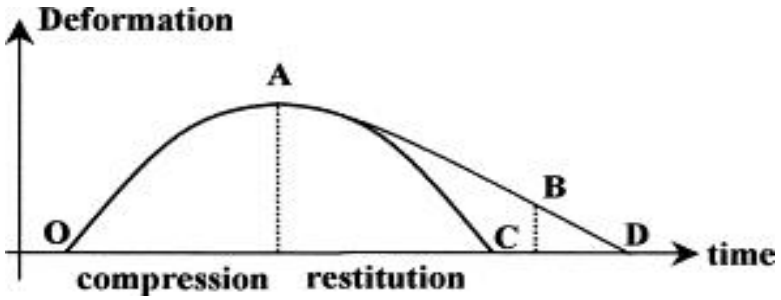

Figure 1.1. Deformation during the impact.

The objective of impact modeling is to determine the after-impact conditions of the system, given its initial (pre-impact) configuration. Because of the complex dependencies on many parameters, one possible solution is to use experimentally measured coefficients.

In order to express the energy loss due to the motion in the normal direction, we can use a coefficient, e, called *restitution coefficient*. This coefficient falls in the interval [0,1]. The case $e=0$ occurs when a perfectly plastic impact takes place, versus the case $e=1$, which corresponds to a perfectly elastic impact. The coefficient of restitution depends on many elements, such as the geometry of the bodies in contact, the approach velocity, and the material properties. Also, the material properties determine the duration of contact and, possibly, friction (sliding or sticking) [9]. Besides the coefficient of restitution defined along normal direction, coefficients along tangential directions may also be defined [3, 4].

Another key aspect of impact and contact dynamics is friction modeling. The relationship used to determine the force of dry friction is the Coulomb's law. It states that the magnitude of the frictional force, F_t, and the magnitude of the normal force, F_n, are related through a coefficient, called *friction coefficient*, and the direction of the vector $\overrightarrow{F_t}$ is always opposite to the relative tangential motion [7]. When there is a sliding, we denote the friction coefficient by μ_d, and we call it *coefficient of dynamic friction*. In this case, the Coulomb's law can be written as $F_t = \mu_d F_n$. When sticking occurs, we denote the friction coefficient by μ_s, and we call it *coefficient of static friction*. For sticking, the Coulomb's law becomes $F_t \leq \mu_s F_n$. The two coefficients take into account the nature of the contact surfaces. Alternative ways to describe the behavior in the tangential directions include the use of tangential coefficient of restitution, based on Newton's model, and the impulse ratio defined as a ratio of tangential impulse to normal impulse. The latter is a generalization of the coefficient of friction and can take into account other tangential forces [3, 4].

If we denote the contact force at impact by $\overrightarrow{F_c}$, then the magnitude P of the impulse can be calculate as the time integral of F_c [34]:

$$P = \lim_{\Delta t \to 0} \int F_c(t) dt \tag{1.1}$$

1.1 Discrete Models

The assumption in the discrete models is that [34]: the impact process is instantaneous and impact forces are impulsive, kinetic variables have discontinuous changes, no displacements occur during the impact, and other finite forces are negligible. This model is more commonly used in rigid body impact problems, and generally in problems where the deformations are minimal and the body is rigid. In order to solve the impact problem, the linear impulse-momentum principle, the angular impulse-momentum principle, and some relations that associate the variables before and after impact, are used.

One relation that links the before and after impact variables on the normal direction is derived from the definition of the coefficient of restitution. In some cases, additional relations are needed on the tangential direction. The relative velocity at the contact point has a normal component and a tangential component. The former is called the *compression* velocity, the later, *sliding* velocity. The principal models of restitution are introduced below.

In Poisson's model [23], the total normal impulse, P_f, is divided into compression impulse, and restitution impulse. We denote the quantities before the impact with small letters, and those ones after the impact with capitals. So, the compression impulse will be denoted by p and restitution impulse by P. Hence, $P_f = p + P$. The coefficient of restitution is defined as:

$$e = \frac{P}{p} \tag{1.2}$$

In Newton's model [36], the coefficient of restitution is defined as:

$$e = -\frac{V_r \cdot \vec{k}}{v_r \cdot \vec{k}} \tag{1.3}$$

where V_r and v_r represent the relative velocity after impact and before impact, respectively.

In Stronge's model, based on the *internal energy dissipation hypothesis* [30], the coefficient of restitution is defined as the square root of the ratio between the energy dissipated during restitution to the energy absorbed during compression. The relation from which we calculate the restitution coefficient can be written as:

$$e^2 = \frac{W}{-w} \tag{1.4}$$

where W and w represent the work done after impact and before impact, respectively.

In order to obtain additional equations, one can pursue either of two possible ways. The first is to define restitution coefficients for the tangential directions. The equations are similar with Equation 1.3:

$$e_x = -\frac{V_r \cdot \vec{i}}{v_r \cdot \vec{i}} \tag{1.5}$$

$$e_y = -\frac{V_r \cdot \vec{j}}{v_r \cdot \vec{j}} \tag{1.6}$$

A third restitution coefficient, for the rotational effects of the impact may also be added [3, 4].

The second way is to relate the quantities on tangential relations with the quantity on normal direction, through some coefficients. Brach [3, 4] introduced the following relations between tangential and normal impulses:

$$P_x = \mu_x P_z \tag{1.7}$$

$$P_y = \mu_y P_z \tag{1.8}$$

Brach model and Poisson model aggree perfectly until sticking occurs.

1.2 Continuous Contact Dynamics Models

These models are useful in cases where the discrete models fail to provide realistic results. For example, if the contact at impact is not instantaneous, a discrete model will overestimate the velocity after impact.

The continuous contact dynamics models can be grouped in two broad categories: *contact force models* and *friction models*. The friction models are suitable for cases when, say, a rigid body hits a rough horizontal barrier. They are more complex than the contact force models, they require more parameters, and they have a less intuitive connection with the physics. Next, three contact force models will be presented.

In the spring-dashpot model, the impact is schematically represented with a linear damper (dashpot) for the dissipation of the energy, in parallel with a linear spring for the elastic behavior [9]. The contact force is defined as [3, 4]:

$$F_n = b\dot{\delta} + k\delta \tag{1.9}$$

where k and b are constants, and δ is the local indentation.

The Hetz's model is a non-linear model useful for the study of the impacts with elastic deformation. In its original form, it does not consider the damping. It considers that the deformation is concentrated in the immediate vicinity of the contact area, does not consider the elastic wave motion, and the total mass of the body moves with the velocity of its centre of mass. The impact force is defined as [2, 9, 12, 14]:

$$F_n = k\delta^m \tag{1.10}$$

where k and m are constants that depend on material properties.

The non-linear damping model combines the previous two models presented here. The impact force is defined as:

$$F_n = b\delta^p\dot{\delta}^q + k\delta^m \tag{1.11}$$

The usual setting is p=m and q=1 [13, 19, 21]. Two important aspects of this kind of models are the fact that damping depends on indentation and that the contact force has no discontinuities at contact and separation. This model has been used and studied by various authors [6, 13, 17, 19, 18, 20, 21, 25, 26, 29, 33, 38].

1.3 Multiple Impacts

In a pioneering study of Goyal et al [10, 11], it was found that when a two-dimensional rod was dropped at a small angle to the ground, the second impact might be as large as twice of the initial impact under some circumstances. For its consequence in applications, their surprising result stirred some interest on this otherwise classical problem.

In the related literature, mathematical issues of one impact or first impact have been considered in a number of papers [5, 15, 31] for rigid body collisions. Even in

single-impact cases, the topic remains a focus of much discussion [8, 32, 34] as many theoretical contact dynamics issues involving frictions started to get resolved recently. Recent attention has been directed to detect and calculate the micro-collisions that occur in a short time interval, when the bodies are allowed to be flexible [29, 39]. These micro-collisions are consequence of the elastic oscillations during one impact, and occur in a relatively short period of time. During the sequence of micro-collisions, the location and posture of the bodies change very little.

The study of multiple-impacts, however, is only an emerging area. Goyal et al [10, 11] used transition matrix method to calculate the clattering sequence and its impacts. In a surprising way, they showed that when a two dimensional rod with uniform density is dropped to the ground at a very small angle, the second impact can be as large as twice of the first impact. Of course, this result is derived based on a number of assumption and simplifications such as full restitution and ignoring the effect of gravity, etc.

1.4 About the Next Chapters

In this thesis, a study of the entire multiple-impact sequence of a two-dimensional rod with/without consideration of gravity, and using a general restitution coefficient is presented in Chapter 2, which presents a prototype problem for cell phone multi-impact dropping by several initial postures. A number of assumptions required in Goyal's study are shown to be valid, and interesting application is found in studying of clattering phenomenon of falling rigid bodies referred in [10, 11]. This model is a first step towards model study for the design and optimization of electronic components for mobile electronic product. Chapter 3 describes the program used in the numerical simulations for the impact problem. Chapter 4 presents a 3D problem of a rectangular plate with zero thickness that collides with the ground. At last, Chapter 5 presents conclusions and discussions.

CHAPTER 2

THE 2D CASE

2.1 Collision Equations for a Falling Rod

The model presented [1, 26] is based on the linear impulse momentum principle, the angular impulse-momentum principle for the rigid body, and some impact parameters that relates the pre- and post-impact variables, such as the coefficient of restitution, which is defined as the ratio of the post-impact relative normal velocity to the pre-impact relative normal velocity at the impact location. The limitation of the model is such that only sliding friction can be allowed. We assume that there is no sticking during the impact process. When sticking does occur, the situation becomes very complex.

We consider two rigid bodies having masses m_1 and m_2 respectively. We denote the initial physical quantities, such as velocities, before collision, in lower cases, and after collision, with capitals. Collision equations are the following:

$$m_i(\overrightarrow{V_i} - \overrightarrow{v_i}) = \overrightarrow{P_i}\,,\ i = 1, 2\,, \tag{2.1}$$

$$\overrightarrow{H_i} - \overrightarrow{h_i} = \overrightarrow{d_i} \times \overrightarrow{P_i}\,,\ i = 1, 2\,, \tag{2.2}$$

where for body $i = 1, 2$, the notations are the following: m_i is the mass, $\overrightarrow{v_i}, \overrightarrow{V_i}$ are the pre- and post- impact velocity, $\overrightarrow{P_i}$ is the impulse, $\overrightarrow{h_i}, \overrightarrow{H_i}$ are the pre- and post- impact angular momentum, $\overrightarrow{d_i}$ is the position vector from the center of mass to the collision contact point.

We can write:

$$\overrightarrow{P_i} = P_{ni}(\overrightarrow{n} + \mu\,\overrightarrow{t}\,)\,, \tag{2.3}$$

where μ is the sliding friction coefficient, $\overrightarrow{n}$, $\overrightarrow{t}$ are the normal and tangential unit vectors of the contact surface

The post-impact relative velocity $\overrightarrow{V_r}$ and pre-impact relative velocity $\overrightarrow{v_r}$ at the collision contact point are related by:

$$\overrightarrow{V_r} \cdot \overrightarrow{n} = -e\overrightarrow{v_r} \cdot \overrightarrow{n}\,, \tag{2.4}$$

where e is the coefficient of restitution.

Related to the center of mass, velocity and angular velocity, $\overrightarrow{V_r}$ and $\overrightarrow{v_r}$ can be written as:

$$\overrightarrow{V_r} = \overrightarrow{V_1} + \overrightarrow{\Omega_1} \times \overrightarrow{d_1} - (\overrightarrow{V_2} + \overrightarrow{\Omega_2} \times \overrightarrow{d_2})\,, \tag{2.5}$$

$$\overrightarrow{v_r} = \overrightarrow{v_1} + \overrightarrow{\omega_1} \times \overrightarrow{d_1} - (\overrightarrow{v_2} + \overrightarrow{\omega_2} \times \overrightarrow{d_2})\,, \tag{2.6}$$

where $\overrightarrow{\omega_i}$ and $\overrightarrow{\Omega_i}$ are the vectors of the pre- and post- impact angular velocities, respectively. For two-dimensional case, $\overrightarrow{\omega_i} = \omega_i\,\overrightarrow{k}$ and $\overrightarrow{\Omega_i} = \Omega_i\,\overrightarrow{k}$, where $\overrightarrow{k}$ is the unit vector normal to the two-dimensional work plane.

The Equations 2.1 – 2.6 form a closed system. Solving the equations above, we derive (see [5] for example):

$$V_{1n} = v_{1n} + \frac{\overline{m}(1+e)q}{m_1} v_{rn}\,, \tag{2.7}$$

$$V_{1t} = v_{1t} + \frac{\mu\,\overline{m}(1+e)q}{m_1} v_{rn}\,, \tag{2.8}$$

$$V_{2n} = v_{2n} - \frac{\overline{m}(1+e)q}{m_2} v_{rn}\,, \tag{2.9}$$

$$V_{2t} = v_{2t} - \frac{\mu\,\overline{m}\,(1+e)q}{m_2} v_{rn}\,, \tag{2.10}$$

$$\Omega_1 = \omega_1 + \frac{\overline{m}(1+e)q(d_{1t} - \mu d_{1n})}{I_1} v_{rn}\,, \tag{2.11}$$

$$\Omega_2 = \omega_2 - \frac{\overline{m}(1+e)q(d_{2t} - \mu d_{2n})}{I_2} v_{rn}\,, \tag{2.12}$$

In the above solution we denoted:

$\overline{m} = \frac{m_1 m_2}{m_1+m_2}$,

$v_{rn} = (v_{2n} - d_{2t}\omega_2) - (v_{1n} + d_{1t}\omega_1)$,

$q = \left[1 + \frac{\overline{m}d_{1t}^2}{I_1} + \frac{\overline{m}d_{2t}^2}{I_2} - \mu\left(\frac{\overline{m}d_{1t}d_{1n}}{I_1} + \frac{\overline{m}d_{2t}d_{2n}}{I_2}\right)\right]^{-1}$,

$e = -\frac{V_{2n}-V_{1n}}{v_{2n}-v_{1n}}$, and

$\mu = \frac{P_t}{P_n}$.

The formula for e is called the Newton's Law of Restitution. The value μ is the relative ratio of impulse, and it reflects the friction coefficient, as long as no sticking is happening during the impact. The terms I_1 and I_2 represent the mass moment of inertia with respect to center of mass, for the two rigid bodies. The subscripts "n" and "t" stand for the normal and tangential components of the velocity vector and the position vectors respectively. The Figure 2.1 shows the position vectors from the mass center to the collision contact point, $\overrightarrow{d_1}$ and $\overrightarrow{d_2}$, together with their normal and tangential components.

If a planar barrier collision occurs, for simplicity, let the moving body be represented by $i = 1$ and the barrier be $i = 2$. All velocities related to body 2 are set to zero. The above approach is now applied to the multiple impacts of a falling rod, see Figure 2.2. In

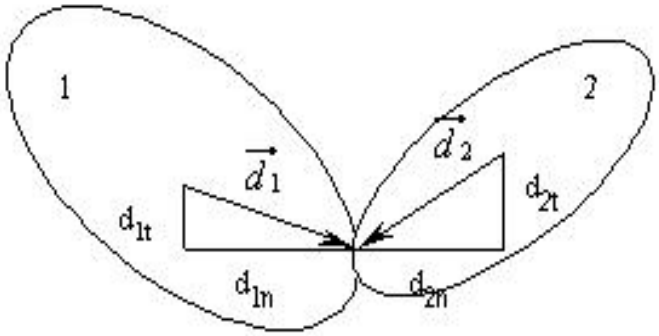

Figure 2.1. Rigid collision between two bodies.

this chapter, we consider a rod with uniform density. The mass of the rod is $m_1 = 1kg$, the length of the rod is l=1m, the moment of inertia of the rod is $I_1 = \frac{1}{12}kgm^2$, the friction coefficient is $\mu = 0$, and the restitution coefficient is $e \in [0, 1]$. The mass of the ground is $m_2 = \infty$.

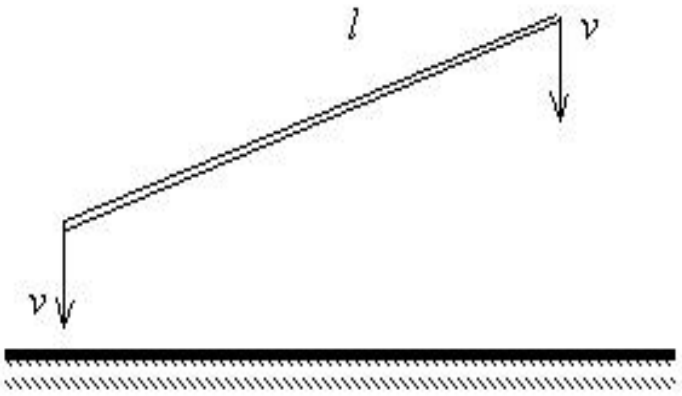

Figure 2.2. A rod colliding with the ground.

Hence, for our case, the Equations 2.1 – 2.6 will reduce to:

$$V_n = v_n + (1+e)q\, v_{rn}\,, \tag{2.13}$$

$$\Omega = \omega + 12(1+e)q\, d_t\, v_{rn} \tag{2.14}$$

with $q = \frac{1}{1+12\, d_t^2}\,, v_{rn} = -(v_n + d_t\, \omega)\,, d_t - \mu\, d_n = d_t = -\frac{\cos\alpha}{2}$

We dropped the index {1,2} in the previous text because we will refer just to the normal and angular velocity of the rod relative to the ground. The tangential velocity remains zero at all the time. Further, we will be interested in the angle at the moment of the impact, and a value of the impulse. We will be having the initial velocity v at the moment right before the first impact, as a unit.

2.2 The First Three Impacts, Disregarding the Effect of Gravity

We assume the impact sequence occurs without gravity. The clattering sequence terminates when the rod will no longer collide with the ground. The impact contact angles at the first three impacts are denoted as $\alpha\,, \beta$, and γ , as shown in Figure 2.3.

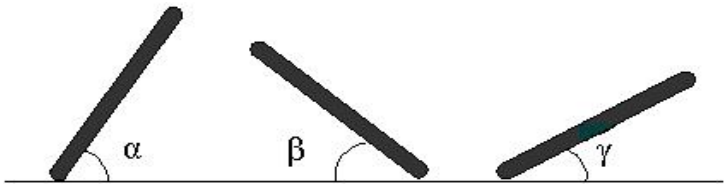

Figure 2.3. The succession of first three impacts of the falling rod. The acute angle between the rod and the ground will be denoted as α, β, γ.

Following from the Equations 2.7 – 2.12, for the first bounce, the quantities can be calculated as:

$$V_n^I = \frac{e - 3\,\cos^2\alpha}{1 + 3\,\cos^2\alpha}\, v\,, \tag{2.15}$$

$$\Omega^I = -\frac{6\,(1+e)\,\cos\alpha}{1+3\,\cos^2\alpha}\,v\,, \tag{2.16}$$

where α is the initial drop angle.

Then the first impact is:

$$P_n^I = V_n^I + v = \frac{1+e}{1+3\,\cos^2\alpha}\,v_{rn}^I\,, \tag{2.17}$$

where:

$$v_{rn}^I = v\,. \tag{2.18}$$

Let us consider h^I the vertical height of the rod's center of mass at first impact, and h^{II} the vertical height at the center of mass at second impact, without considering the gravity. These heights are related to the contact angles as:

$$h^I = \frac{\sin\,\alpha}{2}\,,\; h^{II} = \frac{\sin\,\beta}{2}\,. \tag{2.19}$$

For the second impact, we have the equation:

$$h^I + V_n^I T^I = h^{II}\,. \tag{2.20}$$

where T^I is the duration of airborne. It can be analytically written as

$$T^I = \frac{-(\alpha+\beta)}{\Omega^I}\,. \tag{2.21}$$

We can determine the angle β numerically, for a given initial angle α, using the height relation, so that

$$\sin\,\alpha + \frac{e-3\,\cos^2\,\alpha}{3\,(1+e)\,\cos\,\alpha}\,(\alpha+\beta) = \sin\,\beta\,. \tag{2.22}$$

The new velocities for the second bounce are:

$$V_n^{II} = V_n^I + \frac{1+e}{1+3\,\cos^2\,\beta}\,v_{rn}^{II}\,, \tag{2.23}$$

$$\Omega^{II} = \Omega^I + \frac{6\,(1+e)\,\cos\,\beta}{1+3\,\cos^2\,\beta}\,v_{rn}^{II}\,, \tag{2.24}$$

where:

$$v_{rn}^{II} = -V_n^I - \frac{\cos\,\beta}{2}\,\Omega^I\,. \tag{2.25}$$

This gives the relation between the velocities of first two impacts:

$$V_n^{II} = \frac{-e+3\,\cos^2\,\beta}{1+3\,\cos^2\,\beta}\,V_n^I + \frac{-\frac{1+e}{2}\,\cos\,\beta}{1+3\,\cos^2\,\beta}\,\Omega^I\,, \tag{2.26}$$

$$\Omega^{II} = \frac{-6\,(1+e)\,\cos\,\beta}{1+3\,\cos^2\,\beta}\,V_n^I + \frac{1-3\,e\,\cos^2\,\beta}{1+3\,\cos^2\,\beta}\,\Omega^I\,. \tag{2.27}$$

Hence, by substituting Equations 2.15 – 2.16 into Equations 2.26 – 2.27, we derive

$$V_n^{II} = \frac{-(e-3\,\cos^2\,\alpha)\,(e-3\,\cos^2\,\beta)+3\,(1+e)^2\,\cos\,\alpha\,\cos\,\beta}{(1+3\,\cos^2\,\alpha)\,(1+3\,\cos^2\,\beta)}\,v\,, \tag{2.28}$$

$$\Omega^{II} = \frac{-6\,(1+e)\,(\cos\,\alpha+e\cos\,\beta)\,(1-3\,\cos\,\alpha\,\cos\,\beta)}{(1+3\,\cos^2\,\alpha)\,(1+3\,\cos^2\,\beta)}\,v\,, \tag{2.29}$$

$$v_{rn}^{II} = v + (1+e)\,\frac{-1+3\,\cos\,\alpha\,\cos\,\beta}{(1+3\,\cos^2\,\alpha)}\,v\,. \tag{2.30}$$

The second angle, β, is numerically determined by solving Equation 2.22 using Mathematica [37], and the impulse for second impact is:

$$P_n^{II} = V_n^{II} - V_n^I = \frac{1+e}{1+3\,\cos^2\,\beta}\,v_{rn}^{II}\,. \tag{2.31}$$

The third impact can be calculated in a similar way. The height at the center of mass at the third impact will be

$$h^{III} = \frac{\sin\,\gamma}{2}\,, \tag{2.32}$$

where γ is the third impact angle between the rod and the floor.

At the third impact:

$$h^{II} + V_n^{II} T^{II} = h^{III}\,, \tag{2.33}$$

where $T^{II} = \frac{\beta+\gamma}{\Omega^{II}}$ is the elapsed time between the 2^{nd} and the 3^{rd} impacts. Therefore, we obtain that

$$V_n^{II} T^{II} = \frac{-(e - 3\,\cos^2\,\alpha)\,(e - 3\,\cos^2\,\beta) + 3\,(1+e)^2\,\cos\,\alpha\,\cos\,\beta}{6\,(1+e)\,(\cos\,\alpha + e\cos\,\beta)\,(-1 + 3\,\cos\,\alpha\,\cos\,\beta)}\,(\beta+\gamma)\,, \tag{2.34}$$

Using the relations in Equations 2.23 – 2.24, we obtain the following equation that relates α, β, and γ for a general value of the restitution coefficient e :

$$\sin\,\beta + \frac{-(e - 3\,\cos^2\,\alpha)\,(e - 3\,\cos^2\,\beta) + 3\,(1+e)^2\,\cos\,\alpha\,\cos\,\beta}{3\,(1+e)\,(\cos\,\alpha + e\cos\,\beta)\,(-1 + 3\,\cos\,\alpha\,\cos\,\beta)}\,(\beta+\gamma) = \sin\,\gamma\,. \tag{2.35}$$

Once the angle β is obtained from Equation 2.22 for any given α , the angle γ can be computed numerically using Equation 2.35.

Now we find velocity and angular velocity at the center of mass, V_n and Ω, for the third bounce:

$$V_n^{III} = V_n^{II} + \frac{1+e}{1 + 3\,\cos^2\,\gamma}\,v_{rn}^{III}\,, \tag{2.36}$$

$$\Omega^{III} = \Omega^{II} + \frac{6\,(1+e)\,\cos\,\gamma}{1 + 3\,\cos^2\,\gamma}\,v_{rn}^{III}\,, \tag{2.37}$$

where

$$v_{rn}^{III} = -V_n^{II} + \frac{\cos\,\gamma}{2}\,\Omega^{II}\,. \tag{2.38}$$

Hence,

$$V_n^{III} = \frac{-e + 3\,\cos^2\,\gamma}{1 + 3\,\cos^2\,\gamma}\,V_n^{II} + \frac{\frac{1+e}{2}\,\cos\,\gamma}{1 + 3\,\cos^2\,\gamma}\,\Omega^{II}\,, \tag{2.39}$$

$$\Omega^{III} = \frac{-6\,(1+e)\,\cos\,\gamma}{1 + 3\,\cos^2\,\gamma}\,V_n^{II} + \frac{1 + 3\,(e+2)\,\cos^2\,\gamma}{1 + 3\,\cos^2\,\gamma}\,\Omega^{II}\,. \tag{2.40}$$

To derive an explicit expression of V_n^{III} and Ω^{III} , we substitute the expression of V_n^{II} and Ω^{II} to get:

$$\begin{aligned} V_n^{III} = \frac{1}{(1 + 3\,\cos^2\,\alpha)\,(1 + 3\,\cos^2\,\beta)(1 + 3\,\cos^2\,\gamma)}\cdot \\ ((e - 3\,\cos^2\,\alpha)(e - 3\,\cos^2\,\beta)(e - 3\,\cos^2\,\gamma) - \\ 3\,(1+e)^2\,(\cos\,\alpha\,\cos\,\beta\,(e - 3\,\cos^2\,\gamma) + \\ \cos\,\beta\,\cos\,\gamma\,(e - 3\,\cos^2\,\alpha) + \cos\,\gamma\,\cos\,\alpha\,(e - 3\,\cos^2\,\beta)))\,v\,, \end{aligned} \tag{2.41}$$

$$\begin{aligned} \Omega^{III} = \frac{6\,(1+e)}{(1 + 3\,\cos^2\,\alpha)\,(1 + 3\,\cos^2\,\beta)(1 + 3\,\cos^2\,\gamma)}\cdot \\ (-3\,(1+e)^2\,\cos\,\alpha\,\cos\,\beta\,\cos\,\gamma + \cos\,\gamma\,(e - 3\,\cos^2\,\alpha)(e - 3\,\cos^2\,\beta) + \\ \cos\,\alpha\,(1 - 3\,e\,\cos^2\,\beta)(1 + 3\,(1+e)\,\cos^2\,\gamma) + \\ \cos\,\beta\,(1 + 3\,(2+e)\,\cos^2\,\gamma)(e - 3\,\cos^2\,\alpha))\,v\,. \end{aligned} \tag{2.42}$$

Also, the contact velocity at the 3rd impact is

$$v_{rn}^{III} = v + \frac{(e^2-1) - 3\,(e+1)\,(\cos^2\alpha + \cos^2\beta) - 3\,(e+1)^2\,\cos\alpha\,\cos\beta}{(1+3\,\cos^2\alpha)\,(1+3\,\cos^2\beta)}\,v + 3\,(e+1)\,\frac{\cos\gamma\,(\cos\alpha + e\,\cos\beta)\,(-1+3\,\cos\alpha\,\cos\beta)}{(1+3\,\cos^2\alpha)\,(1+3\,\cos^2\beta)}\,v\,, \tag{2.43}$$

and the impulse at the third impact is:

$$P_n^{II} = V_n^{III} - V_n^{II} = \frac{1+e}{1+3\,\cos^2\gamma}\,v_{rn}^{III}\,. \tag{2.44}$$

We give numerical examples of the formulae for the impact sequence.

For complete restitution ($e = 1$), given a small angle α, the angle β should be less than or equal to α, as long as $1 - 3\,\cos^2 < 0$. We have the equality $\alpha = \beta$ at $\alpha = 54.74^o$. Numerically, there is solution for β until the rod drops on an angle of $\alpha = 58.49^o$. Also, up to this value, the impulse keeps a positive value. There is no solution for β afterwards. From physical point of view, the rod impact sequence ends with just one impact for $\alpha > 58.49^o$.

The impulse for the third impact decreases from $0.5v$ to 0, as the angle α increases from 0^o to 24.79^o. Afterwards, the third impact ceases to exist. The results for full restitution are expressed graphically in Figure 2.4

When α is small, β is roughly half of angle α, and γ is nearly the same as angle α.

When α is small, the second impact is nearly twice of first one, and the third impact is about the same as the first one. The first two impulses become equal at $\alpha = 54.74^o$.

In a separate study of a flexible rod, it was found the restitution $e = 0.5$ is of significance. We show the impact results for half restitution (e =0.5) in a comparison study below.

The results when the restitution coefficient is 0.5 are similar to the full restitution case, although the rebounds at both ends are slower due to energy loss. We can obtain

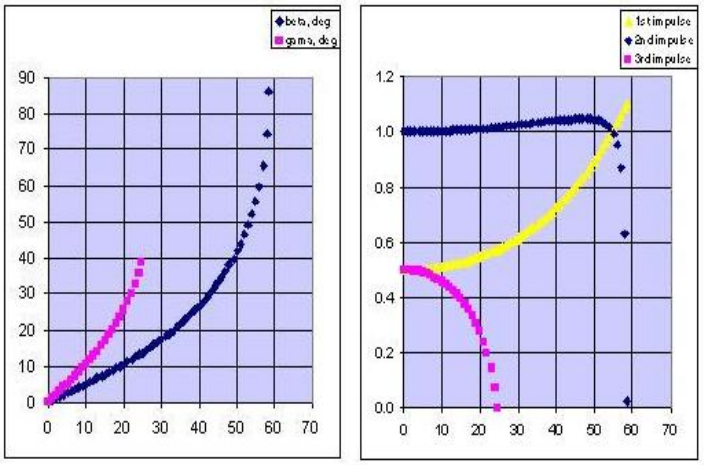

Figure 2.4. (a) The dropping angles at the second and the third impact are shown as functions of the angle α, when e=1. When α is small, β is roughly half of angle α, and γ is nearly the same as angle α; (b) The impulses at the first, second and third impacts are shown as functions of the initial angle α, when e=1. When α is small, the second impact is nearly twice of first one, and the third impact is about the same as the first one.

solution for β until the rod drops on an angle of $\alpha = 67.21^o$. There is no solution for β afterwards.

The impulse for the third impact reaches the zero value for $\alpha = 35.00^o$. The results for half restitution are depicted in Figure 2.5

2.3 The First Three Impacts, with the Gravity

In previous studies [10, 11], it is generally assumed there is no gravity. The validity of such an assumption needs to be checked. In this section, we compare quantitatively the effect of gravity for the impacts sequence. In this case, the rod will fall back again and again because of the gravity. We will still define the clattering sequence as the same number of impact as the case without gravity.

In order to determine the new angles β and γ, we will use the following equations:

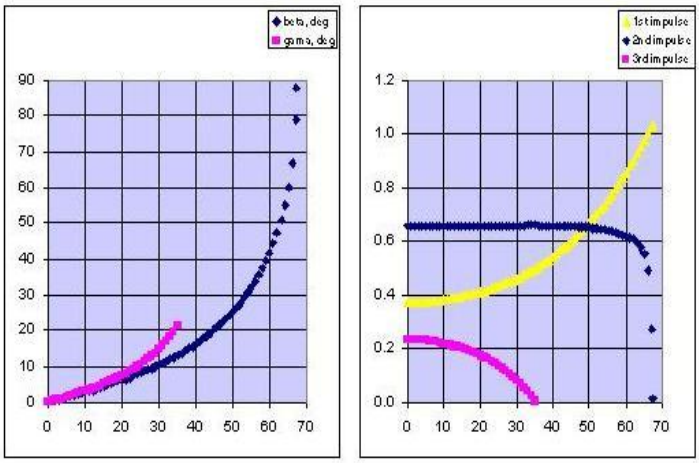

Figure 2.5. (a) The dropping angle at the second and the third impact as function of initial angle, when e=0.5. They are smaller than those for full restitution. The angles where second and third impact terminate are relative higher values when e=0.5; (b) The impulses at the first, second and third impact are presented as a function of initial angle α, when e=0.5. The impact with half restitution involves energy loss during the impact process. Still, the second impact shows much larger impulse when the angle α is relatively small.

$$h^I + V_n^I T^I - \frac{1}{2} g T^{I\,2} = h^{II}\,, \tag{2.45}$$

$$h^{II} + V_n^{II} T^{II} - \frac{1}{2} g T^{II\,2} = h^{III}\,, \tag{2.46}$$

respectively.

By substituting

$$V_n^I = \frac{e - 3\,\cos^2\,\alpha}{1 + 3\,\cos^2\,\alpha}\,v\,, \tag{2.47}$$

and

$$T^I = \frac{-(\alpha+\beta)}{\Omega^I} = \frac{1 + 3\,\cos^2\,\alpha}{6\,(1+e)\,\cos\,\alpha}\,(\alpha+\beta)\,\frac{1}{v}\,, \tag{2.48}$$

in Equation 2.45, the new angle relation for first and second impact is expressed as:

$$\begin{aligned} &\sin\,\alpha + 2(\frac{e - 3\,\cos^2\,\alpha}{6\,(1+e)\,\cos\,\alpha}\,(\alpha+\beta)) - \\ &\frac{1}{2}\frac{g}{v^2}(\frac{1+3\,\cos^2\,\alpha}{6\,(1+e)\,\cos\,\alpha}\,(\alpha+\beta))^2 = \sin\,\beta\,, \end{aligned} \tag{2.49}$$

To derive the relation from second angle to third angle, we use:

$$V_n^{II} = \frac{-(e - 3\,\cos^2\,\alpha)\,(e - 3\,\cos^2\,\beta) + 3\,(1+e)^2\,\cos\,\alpha\,\cos\,\beta}{(1+3\,\cos^2\,\alpha)\,(1+3\,\cos^2\,\beta)}\,v\,, \tag{2.50}$$

and

$$T^{II} = \frac{\beta+\gamma}{\Omega^{II}} = \frac{-(1+3\,\cos^2\,\alpha)\,(1+3\,\cos^2\,\beta)}{6\,(1+e)\,(\cos\,\alpha + e\,\cos\,\beta)\,(1-3\,\cos\,\alpha\,\cos\,\beta)}\,(\beta+\gamma)\,\frac{1}{v}\,. \tag{2.51}$$

Hence:

$$\begin{aligned} &\sin\,\beta + 2(\frac{(e - 3\,\cos^2\,\alpha)\,(e - 3\,\cos^2\,\beta) - 3\,(1+e)^2\,\cos\,\alpha\,\cos\,\beta}{(1+3\,\cos^2\,\alpha)\,(1+3\,\cos^2\,\beta)}\,(\beta+\gamma)) - \\ &\frac{1}{2}\frac{g}{v^2}(\frac{-(1+3\,\cos^2\,\alpha)\,(1+3\,\cos^2\,\beta)}{6\,(1+e)\,(\cos\,\alpha + e\,\cos\,\beta)\,(1-3\,\cos\,\alpha\,\cos\,\beta)}\,(\beta+\gamma))^2 = \sin\,\gamma\,, \end{aligned} \tag{2.52}$$

Using the Equations 2.49 and 2.52, we can find the angles β and γ respectively, given velocity v.

For example, as we are motivated by the cell phone dropping problem, that phone typically starts a free fall from the pocket. Supposing it drops from a height of one meter, we can find v and go on to find the impact angles.

$$\frac{1}{2}g\,t^2 = 1 \;\Rightarrow\; t = \sqrt{\frac{2}{g}}$$

$$v = g\,t \;\Rightarrow\; v = \sqrt{2\,g} \;\Rightarrow\; \frac{g}{v^2} = \frac{1}{2}$$

Hence, by substituting $\frac{1}{2}$ for $\frac{g}{v^2}$ value in the above equations, we find the impact angles and impulses as shown in Figures 2.6-2.7.

As seen in Figure 2.6(a) that the second and third angles change very little for small initial angles by the effect of gravity. Both angles β and γ are smaller in the case with gravity, and also the 2^{nd} and 3^{rd} clattering moment exists for slightly wider ranges of intervals of γ, than in the case when gravity is not considered. The differences $\Delta\beta$ and $\Delta\gamma$ between the cases without and with gravity for the angles β and γ respectively is less than 1^o for almost a half of the interval of existence of β and γ respectively. See Table 2.1 for values of $\Delta\beta$ and $\Delta\gamma$, in percents.

The results for the impulse are similar, in the sense that for the same intervals where $\Delta\beta$ and $\Delta\gamma$ are small, the differences between impulses, ΔP_β and ΔP_γ are less than 1%, where ΔP_β and ΔP_γ denote the relative difference between the impulse at the 2^{nd} and 3^{rd} impact respectively. See Table 2.2. The ranges of the impulses are (1.000 , 1.018) for the 2^{nd} impact, and (0.435, 0.500) for the 3^{rd} impact, as shown in Figure 2.6(b).

In both cases, angles and impulses, the discrepancy is present when the time duration of the airborne is longer. This happens for larger impact angles.

When the restitution coefficient equals 0.5, we also compare the results.

As we observe in Figure 2.7(a-b), that is similar to the cases with total restitution, the angles β and γ change very little for small angles of α by the gravity effect. Both impact angles β and γ are smaller in the case with gravity, and also the 2^{nd} and 3^{rd} clattering moment exists for a wider interval for α than in the case without gravity. The differences $\Delta\beta$ and $\Delta\gamma$ between the cases without and with gravity for the angles β and γ respectively is comparable with the case with total substitution, but since the angles β

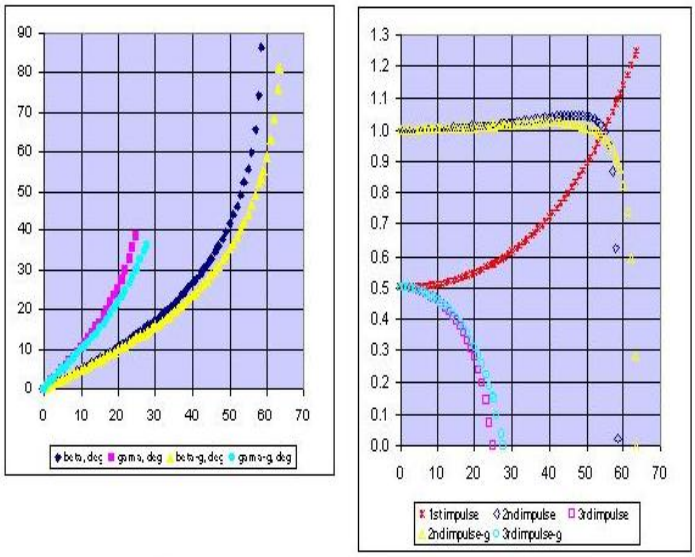

(a) (b)

Figure 2.6. (a) The second and the third angles, for total restitution and in both cases, with and without gravity, as a function of initial angle α; (b) The impulses of the first, second and third impact, for total restitution and in both cases, with and without gravity, are shown as a function of initial angle α.

and γ are smaller in this case, $\Delta\beta$ and $\Delta\gamma$ are bigger as as percentual value. See Table 2.3.

While there is a significative difference between $\Delta\beta$ and $\Delta\gamma$ in the case $e = 1.0$ versus the case $e = 0.5$, ΔP_β and ΔP_γ show very similar behaviour between the two restitution cases. See Table 2.4

Table 2.1. Comparison between the second and third angle of impact, with or without gravity, for the case with total restitution

α,deg	β, deg	γ, deg	β_g, deg	γ_g, deg	$\Delta\beta$, %	$\Delta\gamma$, %
0	0.00	0.00	0.00	0.00	0.00	0.00
5	2.51	5.07	2.47	4.90	1.61	3.21
10	5.08	10.55	4.92	9.87	3.17	6.47
15	7.78	17.02	7.42	15.30	4.65	10.11
20	10.68	25.60	10.04	21.79	6.05	14.89
24.79	13.74	38.90	12.73	29.95	7.31	23.02
25	13.88	.	12.86	30.38	7.36	.
30	17.49	.	15.99	.	8.61	.
35	21.69	.	19.56	.	9.85	.
40	26.75	.	23.76	.	11.18	.
45	33.12	.	28.88	.	12.81	.
50	41.80	.	35.43	.	15.24	.
55	55.74	.	44.44	.	20.26	.
58.49	86.31	.	53.53	.	37.98	.

Table 2.2. Comparison between the second and third impulse, with or without gravity, for the case with total restitution

α,deg	2^{nd} imp.	3^{rd} imp.	2^{nd} imp.-g	3^{rd} imp.-g	$\Delta 2^{nd}$ imp., %	$\Delta 3^{rd}$ imp., %
0	1.0000	0.5000	1.0000	0.5000	0.00	0.00
5	1.0007	0.4899	1.0007	0.4901	0.00	0.05
10	1.0028	0.4574	1.0027	0.4595	0.02	0.46
15	1.0064	0.3947	1.0057	0.4038	0.06	2.32
20	1.0112	0.2767	1.0097	0.3110	0.15	12.38
24.79	1.0169	0.0001	1.0140	0.1557	0.29	.
25	1.0172	.	1.0142	0.1462	0.29	.
30	1.0241	.	1.0188	.	0.53	.
35	1.0317	.	1.0226	.	0.88	.
40	1.0390	.	1.0244	.	1.41	.
45	1.0446	.	1.0218	.	2.18	.
50	1.0429	.	1.0095	.	3.19	.
55	0.9929	.	0.9727	.	2.04	.
58.49	0.0230	.	0.8984	.	.	.

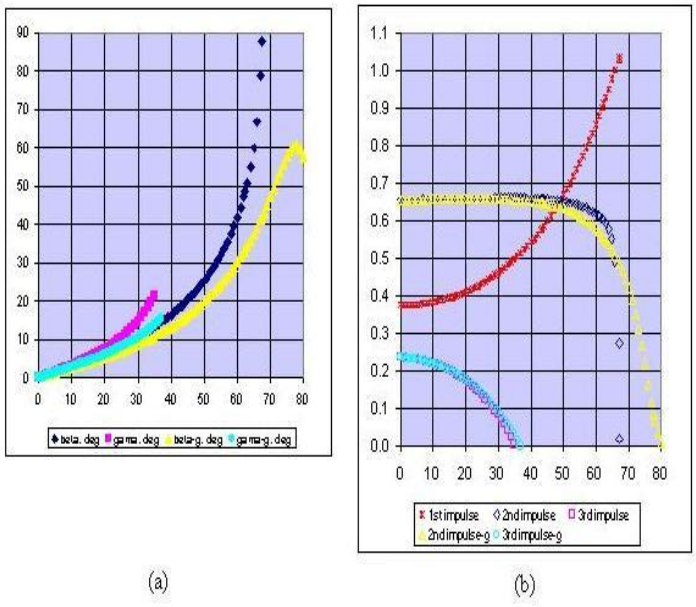

Figure 2.7. (a) The second and the third angle for e=0.5, in both cases, with and without gravity, are shown as a function of initial angle α; (b) The impulse of the first, second and third impact, for e=0.5, in both cases, with and without gravity, is shown as a function of initial angle α.

Table 2.3. Comparison between the second and third angle of impact, with or without gravity, for the case with half restitution

α,deg	β, deg	γ, deg	β_g, deg	γ_g, deg	$\Delta\beta$, %	$\Delta\gamma$, %
0	0.00	0.00	0.00	0.00	0.00	0.00
5	1.44	1.56	1.39	1.48	3.15	4.85
10	2.92	3.22	2.74	2.92	6.12	9.42
15	4.51	5.13	4.11	4.42	8.84	13.82
20	6.26	7.46	5.56	6.10	11.27	18.20
25	8.24	10.49	7.13	8.09	13.40	22.85
30	10.51	14.73	8.91	10.57	15.23	28.24
35	13.20	21.32	10.98	13.77	16.82	35.39
40	16.42	.	13.42	.	18.26	.
43.38	19.00	.	15.35	.	19.22	.
45	20.39	.	16.38	.	19.70	.
50	25.43	.	19.99	.	21.39	.
55	32.15	.	24.50	.	23.79	.
60	41.94	.	30.23	.	27.91	.
62.38	48.71	.	33.51	.	31.19	.
65	59.91	.	37.65	.	37.15	.
67.21	87.80	.	41.62	.	52.60	.

Table 2.4. Comparison between the second and third impulse, with or without gravity, for the case with half restitution

α,deg	2^{nd} imp.	3^{rd} imp.	2^{nd} imp.-g	3^{rd} imp.-g	$\Delta 2^{nd}$ imp., %	$\Delta 3^{rd}$ imp., %
0	0.6563	0.2344	0.6563	0.2344	0.00	0.00
5	0.6564	0.2309	0.6564	0.2309	0.00	0.01
10	0.6569	0.2202	0.6568	0.2204	0.01	0.08
15	0.6577	0.2018	0.6574	0.2024	0.04	0.31
20	0.6587	0.1745	0.6580	0.1762	0.11	0.97
25	0.6597	0.1364	0.6583	0.1404	0.21	2.97
30	0.6605	0.0835	0.6580	0.0932	0.38	11.63
35	0.6608	0.0053	0.6566	0.0311	0.64	.
40	0.6600	.	0.6531	.	1.04	.
43.38	0.6584	.	0.6491	.	1.41	.
45	0.6572	.	0.6465	.	1.64	.
50	0.6513	.	0.6346	.	2.56	.
55	0.6403	.	0.6144	.	4.05	.
60	0.6199	.	0.5805	.	6.35	.
65	0.5508	.	0.5227	.	5.11	.
66	0.4916	.	0.5066	.	-3.04	.
67	0.2744	.	0.4884	.	-78.02	.
67.21	0.0175	.	0.4843	.	.	.

CHAPTER 3

CONTINUOUS CONTACT METHOD

The results obtained by this method [25, 26, 27] are consistent with Goyal's results [10, 11] for the multiple impacts of a rod. The method also gave very good results in simulating the multiple impacts in the case of the dropping of a simplified model of a cell phone. Chapter 4 studies the case of the dropping of a rigid plate to the ground, and compares a direct method with the results obtained by this method. In this case, agreement of both methods is very well. The only significative differences were for very small inclination angles of the plate.

3.1 Rigid Body Dynamics Model

Two sets of coordinate systems are used to describe the displacement and rotation of the rigid body. The global coordinate system (x, y, z) is fixed to the ground, and the local coordinate system (x_0, y_0, z_0), also called body coordinate system, is fixed to the body and has the origin at rigid body's center of mass. Only the gravitational force $\overrightarrow{F_g}$ and the impact contact force $\overrightarrow{F_c}$ are considered.

The equation of unconstrained motion for the rigid body can be written as a set of ordinary differential equations in the following matrix form [24]:

$$M\,\ddot{\overrightarrow{q}} = \overrightarrow{Q_v} + \overrightarrow{Q_e}\,, \tag{3.1}$$

where $\overrightarrow{q} = (\overrightarrow{R}^T, \overrightarrow{\beta}^T)^T$ is the vector of geralized coordinates, $\overrightarrow{R} = (x_c, y_c, z_c)^T$ is the vector of the coordinates of the center of mass with respect to the global coordinate

system, and $\overrightarrow{\beta} = (\beta_0, \beta_1, \beta_2, \beta_3)^T$ is the vector of Euler parameters. The inertia matrix M is given by

$$M = \int_\Omega \rho \begin{pmatrix} I \\ -G'^T \tilde{u}'^T A^T \end{pmatrix} \begin{pmatrix} I & -A\tilde{u}'G' \end{pmatrix} d\Omega \,, \tag{3.2}$$

where the integration is over the entire rigid body, ρ is the density, I is the 3 $\times$ 3 identity matrix, A is the 4 $\times$ 4 transformation matrix, and $\tilde{u}'$ is the skew symmetric matrix obtained from the local coordinates vector $\overrightarrow{u'}$. The matrix G' is a 3 $\times$ 4 matrix expressed in terms of the Euler parameters as

$$G' = 2 \begin{pmatrix} -\beta_1 & \beta_0 & \beta_3 & -\beta_2 \\ -\beta_2 & -\beta_3 & \beta_0 & \beta_1 \\ -\beta_3 & \beta_2 & -\beta_1 & \beta_0 \end{pmatrix} . \tag{3.3}$$

The vectors $\overrightarrow{Q_v}$ and $\overrightarrow{Q_e}$ from the right hand side of Equation 3.1 are define as follows. The first one $\overrightarrow{Q_v}$ represents the vector that absorbs quadratic velocity terms. It is defined as:

$$\overrightarrow{Q_v} = \int_\Omega \rho \begin{pmatrix} I \\ -G'^T \tilde{u}'^T A^T \end{pmatrix} \alpha_v d\Omega \,, \tag{3.4}$$

where $\alpha_v = A\tilde{\omega}'\tilde{\omega}'\overrightarrow{u}' - A\tilde{u}'\dot{G}'\dot{\overrightarrow{\beta}}$ and $\tilde{\omega}'$ is the skew symmetric matrix corresponding to the angular velocity vector ω' of the rigid body in the local coordinate system. The "˙" denotes the derivative with respect to time. The second vector, $\overrightarrow{Q_e}$ is the vector of generalized forces, and it is defined as:

$$\overrightarrow{Q_e} = \begin{pmatrix} (\overrightarrow{Q_e})_R \\ (\overrightarrow{Q_e})_\beta \end{pmatrix} = \begin{pmatrix} \overrightarrow{F_g} + \overrightarrow{F_c} \\ G^T M_c \end{pmatrix} , \tag{3.5}$$

where $G = AG'$. The general force includes the gravitational force $\overrightarrow{F_g}$, and the impact contact force $\overrightarrow{F_c}$ and $\overrightarrow{M_c}$ is the vector of the moment of contact force with respect to the center of mass.

The matrix M is assumed to be positive definite. The Equation 3.1 can be written as

$$\ddot{\overrightarrow{q}} = M^{-1}(\overrightarrow{Q_v} + \overrightarrow{Q_e})\,. \tag{3.6}$$

Further, by introducing the state vector

$$\overrightarrow{U} = \begin{pmatrix} \dot{\overrightarrow{q}} \\ \overrightarrow{q} \end{pmatrix} \tag{3.7}$$

and the load vector

$$\overrightarrow{R} = \begin{pmatrix} M^{-1}(\overrightarrow{Q_v} + \overrightarrow{Q_e}) \\ \dot{\overrightarrow{q}} \end{pmatrix}\,, \tag{3.8}$$

Equation 3.6 can be written as

$$\dot{\overrightarrow{U}} = \overrightarrow{R}\,. \tag{3.9}$$

Equation 3.9 represents a set of ordinary differential equations, which can be solved for given initial conditions. The time integration is accomplished using the third order total-variation-diminishing (TVD) RungeKutta method, see [28].

3.2 Continuous Contact Model

The continuous contact model is well suited for the problem of the collision of a rigid body with the horizontal floor [29, 39]. First, the model allows us to record specific impacts and forces at any particular moment; and second, the viscoelastic parameters

in the model can be used to describe the energy dissipation and elastic reconstitution of the floor. Since the focus is on the trajectory of the impacts rather than micro-collisions, this continuous contact model is well suited. This section contains a brief description of the numerical procedure.

The horizontal ground is modeled as a distributed viscoelastic foundation, which consists of a layer of continuously distributed parallel springs and dampers. Similar ground models have been used in [29, 39] to study the impacts of concentrated masses or of rigid bodies with point impact contact. The surface stiffness is represented by the spring coefficient k_G, and c_G is the ground damping coefficient.

The impact contact force is calculated as the integration of a distributed load over the contact area S in the following form:

$$\overrightarrow{F_c} = \int_S \overrightarrow{f_c} dS \tag{3.10}$$

where $\overrightarrow{f_c} = f_n \overrightarrow{n} + f_t \overrightarrow{t}$ is the vector of the distributed load. The vectors $\overrightarrow{n}$ and $\overrightarrow{t}$ represent the unit vectors in the normal and tangential directions, respectively. As discused in Chapter 1, the components f_n and f_t are determined as follows.

The normal distributed contact load f_n is determined explicitly by the local indentation δ and its rate of change.

$$f_n = (k_G + c_G \dot{\delta})\delta \tag{3.11}$$

The local tangential contact load f_t is computed using Coulomb's law. When sticking occurs, one has

$$f_t \leq \mu_s f_n \tag{3.12}$$

where μ_s is the coefficient of static friction. When sliding occurs, one has

$$f_t = \mu_d f_n \tag{3.13}$$

where μ_d is the coefficient of dynamic (or sliding) friction.

The moment of impact contact force with respect to the center of mass is computed as

$$\overrightarrow{M_c} = \int_S \overrightarrow{m_c} dS \tag{3.14}$$

where $m_c = \tilde{u} f_c$, and $\tilde{u}$ is the skew symmetric matrix corresponding to the local position vector expressed in the global coordinate system.

In this computational model, the three-dimensional rigid body is described by a finite element type mesh that consists of a hexahedral, triangular-based prism, and tetrahedral elements. For impacts between rigid bodies with complex geometries, the impact contact surface is usually irregular. In this dissertation, the ground surface is considered to be flat. For the purpose of impact surface detection, the surface of the rigid body is partitioned by some triangular and quadrilateral surface elements. In the first stage of searching for a surface element that makes contact with the ground, any surface node that contacts with the ground is marked as the impact node, shown as solid dots in Figures 3.1-3.2 [25, 27], where all possible cases are given for the triangular and quadrilateral surface elements. The surface element that contains at least one impact node is marked as the impact element. In the second stage of searching, each edge of the impact element is considered; for any edge with only one end node marked as the impact node, a new impact edge point, shown by empty circles in Figures 3.1-3.2 [25, 27], may be added to that edge to mark the contact and non-contact parts of the edge. All the impact edge points and impact nodes in one surface element will be numbered and linked in proper order to form a closed polygon, as shown by the shaded areas in Figures 3.1-3.2 [25, 27], which is considered as the approximation to the actual impact contact region

in that element. For a triangular surface element, the impact contact region could be a triangle or a quadrangle. For a quadrilateral surface element, the impact contact region could be in the shape of a triangle, quadrangle, or pentagon. After the contact regions are identified, the local contact load $\overrightarrow{f_c}$ on each vertex of the contact region will be calculated based on its local indentation and relative velocity. The local impact moment load m_c on each contact point with respect to the center of mass is also calculated. Finally, total impact contact force and moment are calculated by using Equations 3.10 and 3.14, using the standard Gaussian - Legendre quadrature.

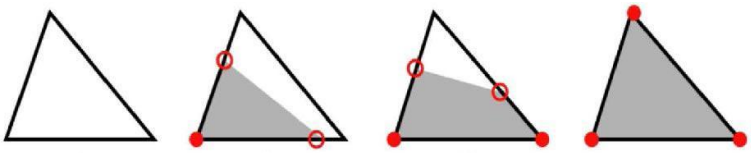

Figure 3.1. Impact contact region for a triangular surface element.

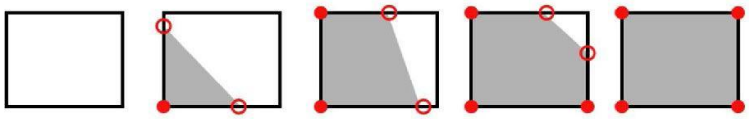

Figure 3.2. Impact contact region for a quadrilateral surface element.

When Coulomb's law is used to calculate the friction force during the impact, if the contact region of the rigid body is sliding on the ground surface during the impact, Equation 3.13 will be used to calculate the tangential friction load.

Assuming that sticking occurs during the impact, the unknown tangential force as part of the solution can be solved with a presumed sticking location. The resultant tangential force will be compared to its maximum value allowed by Coulomb's law; if it

exceeds the maximum possible value, sticking will not happen and a recalculation will be conducted using Equation 3.13 to compute the tangential friction load.

This continuous contact model is able to simulate three-dimensional impact dynamics, though the case for which it is used here is a planar impact problem. The continuous contact model will be used to evaluate the impact contact force in the rigid body dynamics model described in the previous section.

Most of the results were discussed in [25, 26, 27].

CHAPTER 4

RIGID THIN PLATE

After the rod impact problem, the next step is to study a three dimensional problem. For this purpose, when choosing between an analytical and a numerical method, the best suited is the former one. In the case of a body with a complicated geometry, the analytical method may be useless. On the other hand, various numerical simulations may be performed. The program gave good results, matched by results from literature where available, for problems like the study of the clattering impacts of a falling cylindrical rod [26], or the multiple impacts in the case of a simulation of the falling of a simplified phone model [25, 27]. A new case worth to try is that one of a rigid thin plate. This case is also interesting from the analytical point of view because we are able to find closed form solution. The thickness equal to zero is helpful in simplifying the analytical calculations. When running the program, a thickness of 1mm was considered.

The most common case is when the plate falls down to the floor and has a point impact in one of its corners. A more rare situation is that one in which the plate would have a line contact with the flor, falling on one of its sides. This case cannot be treated by using a discrete method, since there is a line contact instead of point contact.

4.1 Collision Equations

For the case of a falling plate, the equations used are:
linear impulse-momentum principle

$$m\,(\overrightarrow{V} - \overrightarrow{v}) = \overrightarrow{P}, \tag{4.1}$$

angular impulse-momentum principle

$$\overrightarrow{H} - \overrightarrow{h} = \overrightarrow{d} \times \overrightarrow{P}, \tag{4.2}$$

pre- and post- impact angular momentum formulas

$$\overrightarrow{h} = I\overrightarrow{\omega}, \tag{4.3}$$

$$\overrightarrow{H} = I\overrightarrow{\Omega}, \tag{4.4}$$

restitution coefficient defined using Newton's restitution law

$$\overrightarrow{V_r} \cdot \vec{n} = -e\overrightarrow{v_r} \cdot \vec{n}, \tag{4.5}$$

relative pre- and post- impact velocity as a sum of linear velocity and rotation

$$\overrightarrow{v_r} = \overrightarrow{v} + \overrightarrow{\omega} \times \overrightarrow{d}\,, \tag{4.6}$$

$$\overrightarrow{V_r} = \overrightarrow{V} + \overrightarrow{\Omega} \times \overrightarrow{d}\,, \tag{4.7}$$

the decomposition of the impulse on the normal direction and two tangentianl directions

$$\overrightarrow{P} = P_z(\vec{k} + \mu_x\vec{i} + \mu_y\vec{j}), \tag{4.8}$$

the definition of the friction coefficients on the tangential directions

$$\mu_x = \mu\cos\eta, \tag{4.9}$$

$$\mu_y = \mu\sin\eta. \tag{4.10}$$

The angle η is measured between the projection of the vector $\overrightarrow{P}$ on the plane $x-y$ and the x axis.

When there is no friction, the system of equations reduces to:

$$V_x = v_x, \tag{4.11}$$

$$V_y = v_y, \tag{4.12}$$

$$m\,(V_z - v_z) = P_z, \tag{4.13}$$

$$I\,(\overrightarrow{\Omega} - \overrightarrow{\omega}) = \overrightarrow{d} \times \begin{pmatrix} 0 \\ 0 \\ P_z \end{pmatrix}, \tag{4.14}$$

$$V_z + (\overrightarrow{\Omega} \times \overrightarrow{d}\,)_z = -e\,(v_z + (\overrightarrow{\omega} \times \overrightarrow{d}\,)_z). \tag{4.15}$$

The inertia in local coordinates is a matrix given by:

$$\bar{I} = \begin{pmatrix} i_{xx} & i_{xy} & i_{xz} \\ i_{yx} & i_{yy} & i_{yz} \\ i_{zx} & i_{zy} & i_{zz} \end{pmatrix}, \tag{4.16}$$

where $i_{xy} = i_{yx}\,, i_{xz} = i_{zx}\,, i_{zx} = i_{xz}$.

The inertia I in the $x-y-z$ system of coordinates is:

$$I = A\,\bar{I}\,A^T\,, \tag{4.17}$$

where A is the transformation matrix of the change of coordonates between local coordinates and $x-y-z$ coordinates

The local system of coordinates has the origin in the center of mass of the plate, the z axis is normal to the surface, and the tangential x and y axes are parallel with the length and width of the plate respectively.

The elements of $\bar{I}$ can be calculated as:

$$i_{xx} = \int_S \rho\,(y^2 + z^2)\,dx\,dy\,, \tag{4.18}$$

$$i_{yy} = \int_S \rho\,(z^2 + x^2)\,dx\,dy\,, \tag{4.19}$$

$$i_{zz} = \int_S \rho\,(x^2 + y^2)\,dx\,dy\,, \tag{4.20}$$

$$i_{xy} = -\int_S \rho\,x\,y\,dx\,dy\,, \tag{4.21}$$

$$i_{yz} = -\int_S \rho\,y\,z\,dx\,dy\,, \tag{4.22}$$

$$i_{zx} = -\int_S \rho\,z\,x\,dx\,dy\,. \tag{4.23}$$

Since the plate does not have thickness, $z = 0$ in the Equations 4.18 – 4.23. The area on which the integration is performed is denoted by S. The local and general systems of coordonates are shown in Figure 4.1.

Hence, the formula of inertia in local coordinates will become:

$$\bar{I} = \frac{m}{12}\begin{pmatrix} l^2 & 0 & 0 \\ 0 & w^2 & 0 \\ 0 & 0 & l^2 + w^2 \end{pmatrix}. \tag{4.24}$$

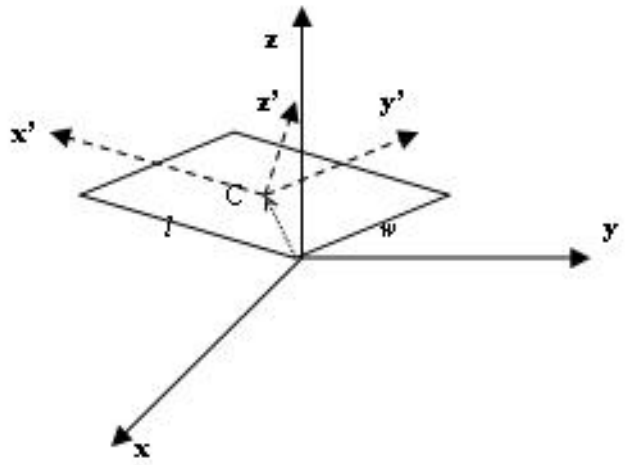

Figure 4.1. The impact of the plate with the ground.

The transformation matrix A used in Equation 4.17 is a product of three rotation matrices A_1 , A_2 , and A_3. These matrices are given by the Euler angles. We denote the Euler angles by ϕ, θ, and ψ. See Figure 4.2 [35]. We say that a body is rotated from its initial position by the Euler angles ϕ, θ, ψ when the following rotations have been performed: first, a rotation of angle ϕ around the z axis, followed by a rotation of angle θ around the new x axis, and by a rotation of angle ψ, around the new z axis. The Euler angles have different names, depending on the area of application. They may be called *azimuth, elevation,* and *tilt* in communications, or *roll, pitch,* and *yaw* in navigation.

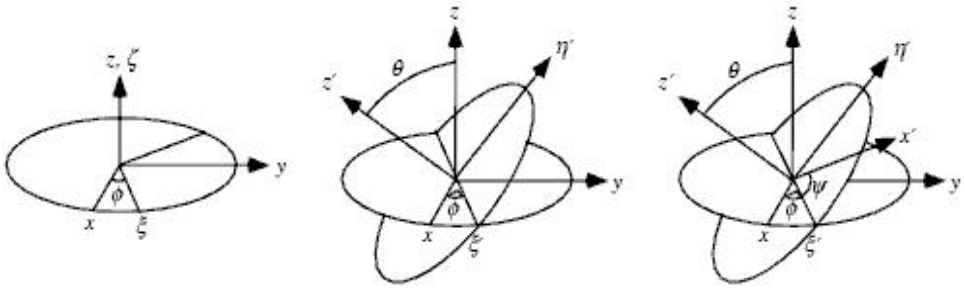

Figure 4.2. Euler angles.

The matrices A_1, A_2, and A_3 used, are the following:

$$A_1 = \begin{pmatrix} \cos\phi & -\sin\phi & 0 \\ \sin\phi & \cos\phi & 0 \\ 0 & 0 & 1 \end{pmatrix}, \phi \in [0, \pi/2] \tag{4.25}$$

$$A_2 = \begin{pmatrix} 1 & 0 & 0 \\ 0 & \cos\theta & -\sin\theta \\ 0 & \sin\theta & \cos\theta \end{pmatrix}, \theta \in [0, \pi/2] \tag{4.26}$$

$$A_3 = \begin{pmatrix} \cos\psi & -\sin\psi & 0 \\ \sin\psi & \cos\psi & 0 \\ 0 & 0 & 1 \end{pmatrix}, \psi \in [-\pi/2, 0] \tag{4.27}$$

Hence, the matrix $A = A_3A_2A_1$ will be

$$A = \begin{pmatrix} \cos\psi\cos\phi - \cos\theta\sin\phi sin\psi & -\cos\psi\sin\phi - \cos\theta\cos\phi sin\psi & \sin\psi\sin\theta \\ \sin\psi\cos\phi + \cos\theta\sin\phi cos\psi & -\sin\psi\sin\phi + \cos\theta\cos\phi cos\psi & -\cos\psi\sin\theta \\ \sin\theta\sin\phi & \sin\theta\cos\phi & \cos\theta \end{pmatrix} \tag{4.28}$$

In the local coordinates, the center of mass C of the plate has the coordinates

$$\begin{pmatrix} \bar{x}_c \\ \bar{y}_c \\ \bar{z}_c \end{pmatrix} = \begin{pmatrix} 0 \\ 0 \\ 0 \end{pmatrix}, \tag{4.29}$$

and the position vector of the body system of coordinates with respect of the general system of coordinates is

$$\overrightarrow{R} = \begin{pmatrix} \frac{l}{2} \\ \frac{w}{2} \\ 0 \end{pmatrix}. \tag{4.30}$$

By multiplying the matrix A with the vector $\overrightarrow{R}$, we get the general coordinates vector. This is

$$\begin{pmatrix} x_c \\ y_c \\ z_c \end{pmatrix} = \begin{pmatrix} \frac{l}{2}(\cos\psi\cos\phi - \cos\theta\sin\phi sin\psi) + \frac{w}{2}(\cos\psi\sin\phi + \cos\theta\cos\phi sin\psi) \\ \frac{l}{2}(-\sin\psi\cos\phi - \cos\theta\sin\phi cos\psi) + \frac{w}{2}(-\sin\psi\sin\phi + \cos\theta\cos\phi cos\psi) \\ \frac{l}{2}\sin\theta\sin\phi - \frac{w}{2}\sin\theta\cos\phi \end{pmatrix} \tag{4.31}$$

The position vector is

$$\overrightarrow{d} = \begin{pmatrix} -x_c \\ -y_c \\ -z_c \end{pmatrix} = -\frac{1}{2}A \begin{pmatrix} l \\ w \\ 0 \end{pmatrix} \tag{4.32}$$

The formulas of the cross products $\overrightarrow{d} \times \overrightarrow{P}$, $\overrightarrow{\Omega} \times \overrightarrow{d}$ and $\overrightarrow{\omega} \times \overrightarrow{d}$ are:

$$\overrightarrow{d} \times \overrightarrow{P} = (\overrightarrow{d} \times \overrightarrow{P})_x \vec{i} + (\overrightarrow{d} \times \overrightarrow{P})_y \vec{j} + (\overrightarrow{d} \times \overrightarrow{P})_z \vec{k} \tag{4.33}$$

where: $(\overrightarrow{d} \times \overrightarrow{P})_x = m(z_c(V_y - v_y) - y_c(V_z - v_z))$, $(\overrightarrow{d} \times \overrightarrow{P})_y = m(x_c(V_z - v_z) - z_c(V_x - v_x))$, $(\overrightarrow{d} \times \overrightarrow{P})_z = m(y_c(V_x - v_x) - x_c(V_y - v_y))$.

$$\overrightarrow{\Omega} \times \overrightarrow{d} = (\Omega_z y_c - \Omega_y z_c)\vec{i} + (\Omega_x z_c - \Omega_z x_c)\vec{j} + (\Omega_y x_c - \Omega_x y_c)\vec{k} \tag{4.34}$$

$$\overrightarrow{\omega} \times \overrightarrow{d} = (\omega_z y_c - \omega_y z_c)\vec{i} + (\omega_x z_c - \omega_z x_c)\vec{j} + (\omega_y x_c - \omega_x y_c)\vec{k} \tag{4.35}$$

If we write the matrices A_1 , A_2 , and A_3 as $A_1(\phi)$, $A_2(\theta)$, and $A_3(\psi)$ respectively, then the matrix A will be $A = A_3(\psi)A_2(\theta)A_1(\phi)$. Hence, the inverse A^{-1} can be written as:

$$A^{-1} = A_3(-\psi)A_2(-\theta)A_1(-\phi) = A_3(\psi)^T A_2(\theta)^T A_1(\phi)^T = A^T \tag{4.36}$$

The inverse of matrix I is

$$I^{-1} = (A\bar{I}A^T)^{-1} = A\bar{I}^{-1}A^T \tag{4.37}$$

Since

$$(\overrightarrow{\Omega} - \overrightarrow{\omega}) = I^{-1}\overrightarrow{d} \times \overrightarrow{P}, \tag{4.38}$$

using Equation 4.1, we derive

$$\overrightarrow{\Omega} - \overrightarrow{\omega} = mI^{-1}(\overrightarrow{d} \times (\overrightarrow{V} - \overrightarrow{v})). \tag{4.39}$$

Using Equations 4.3, 4.5, 4.7, 4.34 and 4.35, we get

$$V_z + (\Omega_y x_c - \Omega_x y_c) = -e(v_z + (\omega_y x_c - \omega_x y_c))\,. \tag{4.40}$$

Hence, we can express

$$V_z - v_z = -(1+e)v_z - e(\omega_y x_c - \omega_x y_c) - (\Omega_y x_c - \Omega_x y_c)\,. \tag{4.41}$$

Also, from Equations 4.1 and 4.8,

$$V_x - v_x = \mu \cos\eta (V_z - v_z) \tag{4.42}$$

$$V_y - v_y = \mu \sin\eta (V_z - v_z) \tag{4.43}$$

We denote the inverse of the inertia matrix in general coordinates, by:

$$I^{-1} = \begin{pmatrix} j_{xx} & j_{xy} & j_{xz} \\ j_{yx} & j_{yy} & j_{yz} \\ j_{zx} & j_{zy} & j_{zz} \end{pmatrix} \tag{4.44}$$

The x, y, and z components of the difference $\overrightarrow{\Omega} - \overrightarrow{\omega}$ are:

$$\Omega_x - \omega_x = m(\mu \cos\eta (j_{xz} y_c - j_{xy} z_c) + \mu \sin\eta (j_{xx} z_c - j_{xz} x_c) + (j_{xy} x_c - j_{xx} y_c))(V_z - v_z) \tag{4.45}$$

$$\Omega_y - \omega_y = m(\mu \cos\eta (j_{yz} y_c - j_{yy} z_c) + \mu \sin\eta (j_{yx} z_c - j_{yz} x_c) + (j_{yy} x_c - j_{yx} y_c))(V_z - v_z) \tag{4.46}$$

$$\Omega_z - \omega_z = m(\mu \cos\eta (j_{zz} y_c - j_{zy} z_c) + \mu \sin\eta (j_{zx} z_c - j_{zz} x_c) + (j_{zy} x_c - j_{zx} y_c))(V_z - v_z) \tag{4.47}$$

The six Equations 4.41, 4.42, 4.43, 4.45, 4.46, and 4.47 contain six unknowns, so we can proceed on solving a 6×6 linear system. In fact, if we rewrite Equation 4.5, we may be able to calculate $V_y - v_y$ without involving Ω_x or Ω_y , and then use it in Equations 4.45, 4.46, and 4.47.

$$((\overrightarrow{V} - \overrightarrow{v}) + \overrightarrow{v} + (\overrightarrow{\Omega} - \overrightarrow{\omega}) \times \overrightarrow{d} + \overrightarrow{\omega} \times \overrightarrow{d}) \cdot \vec{k} = -e(\overrightarrow{v} + \overrightarrow{\omega} \times \overrightarrow{d}) \cdot \vec{k} \tag{4.48}$$

This is:

$$((\overrightarrow{V} - \overrightarrow{v}) + (\overrightarrow{\Omega} - \overrightarrow{\omega}) \times \overrightarrow{d}) \cdot \vec{k} = -(e+1)(\overrightarrow{v} + \overrightarrow{\omega} \times \overrightarrow{d}) \cdot \vec{k} \tag{4.49}$$

where

$$\overrightarrow{V} - \overrightarrow{v} = \begin{pmatrix} \mu\cos\eta \\ \mu\sin\eta \\ 1 \end{pmatrix} (V_z - v_z) \ ,$$
$$\overrightarrow{\Omega} - \overrightarrow{\omega} = mI^{-1}\overrightarrow{d} \times (\overrightarrow{V} - \overrightarrow{v}) \, .$$

Equation 4.49 becomes:

$$(V_z - v_z)\left(\begin{pmatrix} \mu\cos\eta \\ \mu\sin\eta \\ 1 \end{pmatrix} + mI^{-1}\left(\overrightarrow{d} \times \begin{pmatrix} \mu\cos\eta \\ \mu\sin\eta \\ 1 \end{pmatrix} \times \overrightarrow{d}\right)\right) \cdot \overrightarrow{k} = -(e+1)(\overrightarrow{v} + \overrightarrow{\omega} \times \overrightarrow{d}) \cdot \overrightarrow{k} \tag{4.50}$$

where

$$I^{-1}\left(\overrightarrow{d} \times \begin{pmatrix} \mu\cos\eta \\ \mu\sin\eta \\ 1 \end{pmatrix} \times \overrightarrow{d}\right) = \begin{pmatrix} j_{xx} & j_{xy} & j_{xz} \\ j_{yx} & j_{yy} & j_{yz} \\ j_{zx} & j_{zy} & j_{zz} \end{pmatrix} \begin{pmatrix} \mu\cos\eta(y_c^2 + z_c^2) - x_c(\mu\sin\eta y_c + z_c) \\ \mu\sin\eta(z_c^2 + x_c^2) - y_c(z_c + \mu\cos\eta x_c) \\ (x_c^2 + y_c^2) - z_c(\mu\cos\eta x_c + \mu\sin\eta y_c) \end{pmatrix} . \tag{4.51}$$

Finally, we can write:

$$V_z - v_z = -\frac{e+1}{\alpha_z}(v_z - \omega_y x_c + \omega_x y_c) \tag{4.52}$$

where

$$\alpha_z = 1 + m(j_{zx}(\mu\cos\eta(y_c^2 + z_c^2) - x_c(\mu\sin\eta y_c + z_c)) + j_{zy}(\mu\sin\eta(z_c^2 + x_c^2) - y_c(z_c + \mu\cos\eta x_c)) + j_{zz}((x_c^2 + y_c^2) - z_c(\mu\cos\eta x_c + \mu\sin\eta y_c)))$$

Now we can calculate V_z function of v_z, since all other data are known. Then, V_x, V_y , Ω_x, Ω_y, and Ω_z will follow from similar formula.

Figure 4.3 shows a graphical comparison of the results obtained through numerical simulation (the continuous contact method) and the results obtained through the analytical method (discrete contact method).

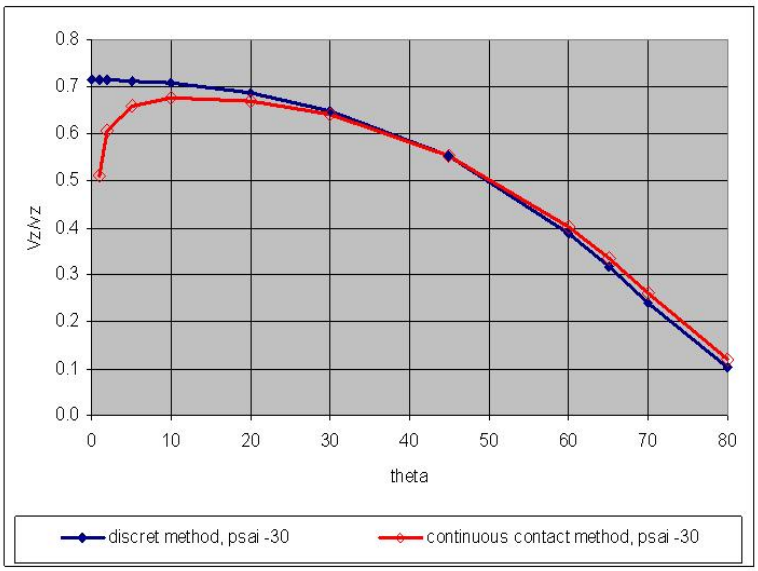

Figure 4.3. A comparison between continuous contact method and discrete method for different initial positions of the plate. For any ϕ, θ from 0 to 80 degrees, and ψ equal to -30 degrees.

The best match of the results is for the angle θ between 20^o and 45^o. After 45^o, the results match less and less. The worst match is for the angle θ between 0^o and 20^o, especially for the angles less 5^o.

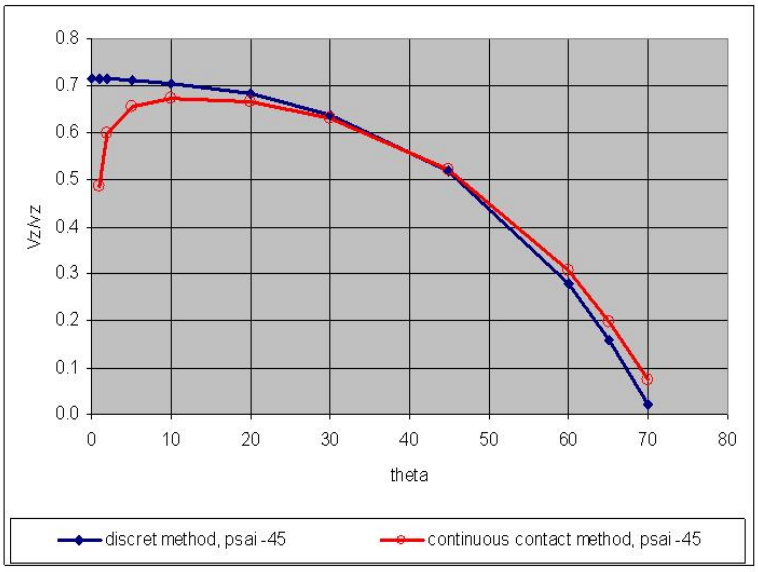

Figure 4.4. A comparison between continuous contact method and discrete method for different initial positions of the plate. For any ϕ, θ from 0 to 80 degrees, and ψ equal to -45 degrees.

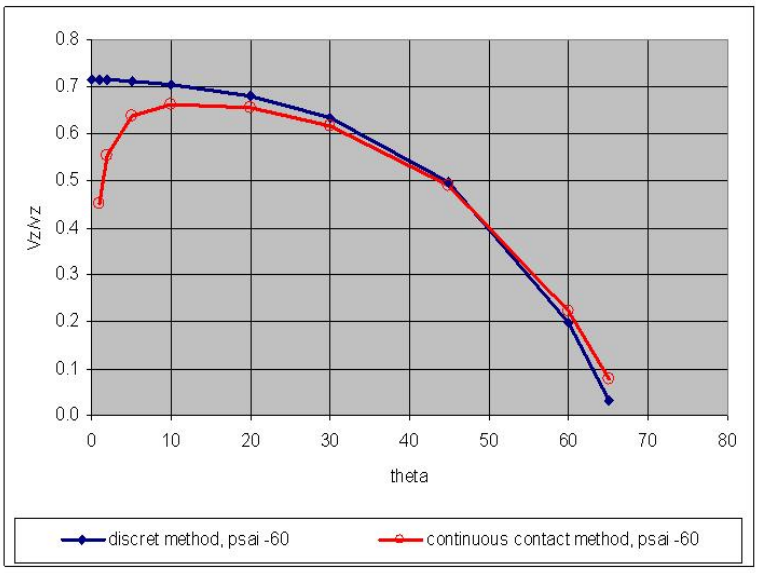

Figure 4.5. A comparison between continuous contact method and discrete method for different initial positions of the plate. For any ϕ, θ from 0 to 80 degrees, and ψ equal to -60 degrees.

CHAPTER 5

DISCUTIONS

The results of the study of the multiple impacts of rod with uniformly distributed mass confirm the results of Goyal et al [10, 11] that if a rod falls to the ground in a small angle, then its clattering impact series has a much larger second impact than the initial one. Furthermore, this analytic study finds that same phenomenon is happening to angles as large as 54 degree. In realistic situations, the range might be smaller when energy dissipation and softness of the ground are included in consideration as we indicated in the case study of $e = 0.5$.

In both situations of $e = 0.5$ and $e = 1.0$ without gravity, there is no 4^{th} impact. With gravity, the 4^{th} impact will occur, but it does not belong to the same clattering sequence of the first three impacts. So we restrict our discussion to first three impacts.

Through the comparison study, one can find that gravity plays only a minor role in our clattering problems. Though friction is not considered in this study, we understand that the fiction is a much complex issues. Some initial study indicated that with a certain friction on the ground, when drop angle is small, sticking might occur during the impact process. If the initial rotation is also included, then there is possibility of revered sliding as well as sticking, as discussed in [34, 27].

For the case of the plate collinding with the ground, the best match of the results is for the angle θ between 20^o and 45^o. After 45^o, the results match less and less. This happens because a bigger aiborne duration between one impact and the next one. The worst match is for the angle θ between 0^o and 20^o, especially for the angles less 5^o. The dynamics in this case can be more complicated. For angles less than 5^o, the contact is

pointwise for the discrete method, versus area contact for the continuous contact method. As shown in [25, 27], the second impact may be more than twice the first one. This is a good reason in favour of studying the multiple impact problems.

REFERENCES

[1] Badiu, F., Su, J., Shan, H., Zhu, J., and Xu, L., *An analysis of clattering impacts of a falling rod.*, Nonlinear Dynamics and Systems Theory 6(1) (2006), pp. 49-62.

[2] Barkan, P., *Impact design. Mechanical Design and Systems Handbook, Section 31.*, McGraw-Hill, New York (1974).

[3] Brach, R.M., *Mechanical Impact Dynamics: Rigid Body Collisions.*, John Wiley and Sons, New York (1991).

[4] Brach, R.M., *Formulation of rigid body impact problems using generalized coefficients.*, International Journal of Engineering Science 36 1 (1998), pp. 61-71.

[5] Brach, R.M., *Rigid-body collision.*, ASME J. Appl. Mech.56, (1989), pp 133-139.

[6] Deguet, A., Joukhadar A., and Laugier, C., *A collision model for deformable bodies.*, IEEE International Conference on Robotics and Automation 1 (1998), pp. 636-641.

[7] De Jalon J.G., and Bayo, E., *Kinematic and Dynamic Simulation of Multi-body Systems–The Real Time Challenge.*, Mechanical Engineering Series., Springer-Verlag, New York (1993).

[8] Gilardi G., and Sharf, I., *Literature survey of contact dynamics modeling.*, Mechanism and Machine Theory, 37 (2002) pp. 1213-1239.

[9] Goldsmith, W., *Impact: The Theory and Physical Behavior of Colliding Solids.*, Edward Arnold Publishers Ltd, London (1960).

[10] Goyal, S., Papadopoulos J. M., and Sullivan, P.A., *The dynamics of clattering I: equation of motion and examples.*, ASME Journal of dynamic systems, measurement and control. 120 (1998), pp 83-93.

[11] Goyal, S., Papadopoulos J. M., and Sullivan, P.A., *The dynamics of clattering II: equation of motion and examples.*, ASME Journal of dynamic systems, measurement and control. 120 (1998), pp 94-101.

[12] Hertz, H., *Miscellaneous papers.*, In: H. Hertz, Editor, Jones and Schott, London (1896).

[13] Hunt K.H., and Crossley, F.R.E., *Coefficient of restitution interpreted as damping in vibroimpact.*, Journal of Applied Mechanics 42, Series E (1975), pp. 440-445

[14] Johnson, K.L., *Contact Mechanics.*, Cambridge University Press, Cambridge (1985).

[15] Keller, J.B., *Impact with friction.*, ASME Journal of Applied Mechanics 53, (1986), pp 1-4.

[16] Kim, S.W., *Contact Dynamics and Force Control of Flexible Multi-Body Systems.*, Ph.D. Thesis, Department of Mechanical Engineering, McGill University, Montreal (1999).

[17] Kraus, P.R., and Kumar, V., *Compliant contact models for rigid body collisions.*, IEEE International Conference on Robotics and Automation 2 (1987), pp. 1382-1387.

[18] Lee, T.W., and Wang, A.C., *On the dynamics of intermittent-motion mechanisms, Part 1: Dynamic model and response.*, Journal of Mechanisms, Transmissions, and Automation in Design 105 (1983), pp. 534-540.

[19] Lankarani, H.M., and Nikravesh, P.E., *A contact force model with hysteresis damping for impact analysis of multi-body systems.*, Journal of Mechanical Design 112 (1990), pp. 369-376.

[20] Ma, O., *Contact dynamics modeling for the simulation of the space station manipulators handling payloads.*, IEEE International Conference on Robotics and Automation 2 (1995), pp. 1252-1258.

[21] Marhefka, D.W., and Orin, D.E., *A compliant contact model with nonlinear damping for simulation of robotic systems.*, IEEE Transactions on Systems, Man, and Cybernetics–Part A: Systems and Humans 29 6 (1999), pp. 566-572

[22] Riley W.F., and Sturges, L.D., *Engineering Mechanics Dynamics.*, John Wiley and Sons, New York (1996).

[23] Routh, E.T., *Dynamics of a System of Rigid Bodies.*, MacMillan & Co, London (1905).

[24] Shabana, A., *Computational Dynamics.*, 2^{nd} edition, John Wiley & Sons, New York (2000).

[25] Shan, H., Su, J., Badiu, F., Zhu, J., and Xu, L., *Modeling and simulation of multiple impacts of faling rigid bodies.*, Mathematics and Computer Modeling 43 (2006), pp. 592-611.

[26] Shan, H., Su, J., Badiu, F., Zhu, J., and Xu, L., *Multiple impact dynamics of a falling rod and its numerical solution.*, The 8th International Conference on Integral Methods in Science and Engineering (IMSE 2004), August 2-4, Orlando, FL (2004)

[27] Shan, H., Su, J., Zhu, J., and Xu, L., *Three dimensional modeling and simulation of a falling electronic device.*, ASME Journal of Computational and Nonlinear Dynamics, 2(1) (2006), pp. 22-31.

[28] Shu, C.W. and Osher, S., *Efficient implementation of essentially non-oscillatory shock-capturing schemes.*, Journal of Computational Physics 75 (1988) pp. 439471.

[29] Stoianovici, D., and Hurmuzlu, Y., *A critical study of the applicability of rigid-body collision theory.*, Journal of Applied Mechanics 63 (1996), pp. 307-316.

[30] Stronge, W.J., *Unraveling paradoxical theories for rigid body collisions.*, Journal of Applied Mechanics 58 (1991), pp. 1049-1055.

[31] Stronge, W.J., *Rigid-body collision with friction.*, Proceeding of Royal society, London, A431,(1990), pp 169-181.

[32] Stewart, D.E., *Rigid-body dynamics with friction and impact.*, SIAM Review, 42, (2000), pp 3-39

[33] Vukobratovic, M.K., and Potkonjak, V., *Dynamics of contact tasks in robotics. Part I: General model of robot interacting with environment.*, Mechanism and Machine Theory 34 (1999), pp. 923-942.

[34] Wang, Y., and Mason, M.T., *Two dimensional rigid-body collisions with friction.*, ASME Journal of Applied Mechanics 59 (1992), pp. 635-642

[35] Weisstein, E.W., *Euler Angles.*, From MathWorld–A Wolfram Web Resource. http://mathworld.wolfram.com/EulerAngles.html.

[36] Whittaker, E.T., *A Treatise on the Analytical Dynamics of Particles and Rigid Bodies.*, Cambridge University Press, Cambridge (1904).

[37] Wolfram, S., *The MATHEMATICA Book.*, Forth edition, Cambridge University Press, Cambridge (1999).

[38] Yigit, A.S., Ulsoy, A.G., and Scott, R.A., *Spring-dashpot models for the dynamics of a radially rotating beam with impact.*, Journal of Sound and Vibrations 142 (1990), pp. 515-525.

[39] Yigit, A.S., Ulsoy, A.G., and Scott, R.A., *Dynamics of radially rotating beam with impact, Part 1: Theoretical and computational model.*, Journal of Vibration and Acoustics, 12 (1990), pp. 65-70.

BIOGRAPHICAL STATEMENT

Florin V. Badiu (FVB) was born on April 6, 1974, in Campina, Prahova County, Romania. He graduated with the Bachelor of Science degree in 1997, on a Pure Mathematics track, form University of Bucharest, in Romania.

After the college graduation, FVB came back to his hometown area and worked in the local petroleum industry. He worked for almost a year, as a Mathematician, at Petrostar. After that, he joined Petrom (the biggest company in Romania), again on a Mathematician position.

FVB started his graduate studies in Mathematics at The University of Texas at Arlington, in January 2002. In December 2003 he graduated with a Master of Science degree. Now, in August 2007, he is graduating with his Doctor of Philosophy degree. His current research is on rigid body impact problems. His work for the dissertation was partially founded by a grant from Nokia.

FVB is a member of American Mathematical Society, Society of Mathematical Sciences from Romania, Society of Petroleum Engineers, and the local chapter of Mathematical Association of America.